

Effects of Joule Heating and Variable Porosity on Non-Newtonian Nanofluid Flow Between Vertical Plates

***¹Agunbiade, S.A., ²Oyekunle, T.L., ³Akolade, M.T., ¹Ayinde, S.A., ¹Uka, U.A., ⁴Ishola, C.Y., ¹Alamu-Awoniran, F.H., & ⁵Raji, R.A.**

¹Department of Basic Sciences, Babcock University, Ogun State, Nigeria.

²Department of Mathematics, Faculty of Physical Sciences, University of Ilorin, Nigeria.

³Department of Computer Science, Lead City University, Ibadan, Nigeria.

⁴Department of Mathematics, National Open University of Nigeria, Abuja.

⁵Department of Social Sciences, Osun State Polytechnic, Ire, Nigeria.

***Corresponding author email:** agunbiades@babcock.edu.ng

Abstract

The impacts of permeability and variable porosity on non-Newtonian nanofluid within flat bounded plates is considered in this work. The spatial variations is emphasised in the analysis on the behaviour of the fluid with nanofluid impact resulted in complex characteristics flow. The non-Newtonian and variable porosity reflect in the formulation of the governing equations as ordinary differential equations. The solution of these equations are obtained using Legendre collocation method which is an accurate and efficient method. The results revealed the impacts of permeability and variable porosity in the presence of joule heating on the flow, heat transfer and generally system performance providing useful insights for industrial processes dealing with non-Newtonian nanofluids particularly in a porous media. Considering comparative analysis, the results show that there is consistency with previous studies when embedded parameters are zeros.

Keywords: Legendre collocation method; Variable porosity; Joule heating; Nanofluid; Non- Newtonian; Free Convection.

Introduction

Natural buoyancy forces caused by density variations as a result of fluids temperature differences lead to natural convective fluid flow. Natural convective fluid flow does not required external devices such as pumps or fan; it occurs naturally unlike forced convection. This phenomenon is essential in various natural and industrial processes, such as atmospheric circulation, oceanic currents, and engineering heat transfer applications. The effectiveness of heat and mass transfer in free convection is determined by factors like the temperature gradient, fluid characteristics, and system geometry. Due to its relevance in fluid mechanics, many researchers such as Jha and Ajibade (2015) and Rajagopal et al (1985) considered natural convection many decades ago and recently by Karem and Hussein (2022). Furthermore, Rajdeep et al. (2023) considered in a porous medium free Convective Radiative Flow in the presence of Soret effects. The result revealed that both velocity and temperature were enhanced by Soret effect.

Variable porosity in fluid flow refers to the condition where the porosity of the medium, or the fraction of the volume that is void space through which the fluid can move, changes spatially or temporally within the flow domain. This variation can significantly influence the behaviour of fluid flow, as it affects the permeability of the medium, which in turn impacts the velocity, pressure distribution, and overall flow dynamics. In porous media, regions with higher porosity allow easier fluid passage, resulting in increased flow rates, while areas with lower porosity restrict fluid

movement, leading to pressure build-up and altered flow patterns. Variable porosity is a critical consideration in fields such as hydrogeology, petroleum engineering, and chemical process design, where understanding and managing flow through heterogeneous porous materials is essential for predicting system behaviour and optimizing performance. Hence, Bidyut et al. (2020) examined mixed convective MHD in porous Darcy medium. The result revealed that porous parameter increases the skin friction coefficient. Variable porosity and viscosity effects in the presence of Soret and Dufour was investigated by Reddy et al. (2017). Subbarao et al. (2016) explored influence of Thermal radiation in a regime with variable porosity. They reported that velocity accelerated with increase in porosity. Viscous dissipation impact Rivlin-Ericksen fluid via a porous plates was studied by Agunbiade and Dada (2019). Hassana et al. (2018), Verma et al. (2021), Oyekunle et al. (2023) studied nanofluid flow via Porous medium.

Furthermore, Khan et al. (2022) considered influence of Hall current in flow of bioconvection Oldroyd-B nanofluid. They reported that nanoparticles concentration decelerated with an hike in Schmidt number values. While Ayub et al. (2022) examined viscous fluid MHD rotational flow in the presence of Hall effect and slip condition via porous media. Zayyanu et al. (2022) investigated Free Convection with impacts of Porosity. The result shown that the present of porosity slowed down the velocity profiles.

The non-Newtonian fluids involving changes in viscosity with respect to applied stress, has various industrial applications and as a result, attracted the attention of technologists, scientists and researchers. Newtonian fluids has constant viscosity not minding the applied force, while non-Newtonian behaviours differently; it experiences shear thinning and shear thickening for decreased and increased viscosity respectively due to stress. These properties are exploited in industries such as pharmaceuticals, food processing, and cosmetics, where fluid behaviour control is essential. For example, the toothpaste formulation which enables it to stay firm on the toothbrush but flows easily while brushing is non-Newtonian fluid dynamics application. Technologists and researchers are working tirelessly on new applications and formulations, for instance, in biomedical devices and advanced manufacturing techniques. In these area, non-Newtonian fluids properties are tailored for performance and functionality enhancement.

Non-Newtonian nanofluid characteristics flow in flat infinite bounded vertical flat plates was analyzed by Peyman et al. (2019). They reported that magnetic force has adverse effects on velocity, Skin friction coefficient and thermal profiles. Amel and Mohamed (2020) investigated third grade non-Newtonian nanofluid with Joule heating via porous materials. Agunbiade et al. (2023) studied influence of dissipation on Maxwell Fluid over porous stretched sheet with material time relaxation. Time is required in heat tranfer through the mediums as a result of material relaxation.

Thermal radiation importance can be seen in its applications in science, industry and technology which gives account on heat transfer. This kind of heat transfer is known as transfer of heat as electromagnetic waves which is useful for high temperature or processes where convection and conduction is insufficient. Thermal radiation is significant in optimizing energy efficiency in Industrial applications like combustion systems, furnaces and high-temperatures reactors. Hence, effects of radiation on non-Newtonian nanofluids and third-grade Nanofluid were examined by Anas et al. (2021) and Asia et al. (2024) respectively. Although the previously discussed research has examined different facets of non-Newtonian nanofluid flow, it has not covered the interactive effects of variable porosity and permeability alongside Joule heating in bounded flat vertical plates. This research aims to address this oversight by exploring these combined effects and providing fresh insights into the behavior of non-Newtonian nanofluids under these circumstances.

Mathematical analysis

The study considered the impacts of variable porosity and joule heating on the flow of non-Newtonian nanofluids between infinite flat plates in the presence of permeability. The plates are considered parallel, with a distance of $2h$ between them. Assumptions of this model include: (i) The flow is steady, incompressible, and laminar. (ii) Variable porosity and permeability are functions of Spatial coordinates. (iii) Thermal equilibrium between base fluid and nanoparticles is assumed. Mathematical modeling involves the Navier-Stokes equations modified for non-Newtonian fluids.

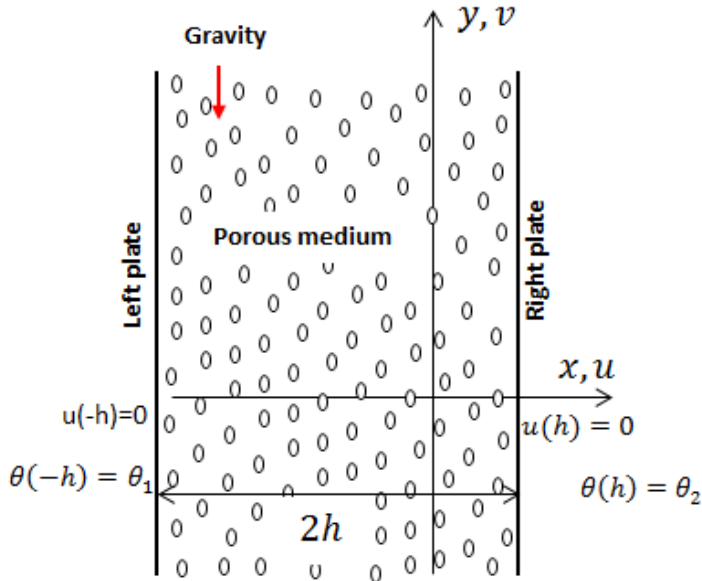


Figure 1: Stagnation Point flow model configuration with Darcy dissipation.

The governing equations in dimensional form, including the momentum and energy equations (Hussein, 2022) are:

$$\mu_{nf} \frac{d^2u}{dx^2} + 6\beta_d \left(\frac{du}{dx} \right)^2 \frac{d^2u}{dx^2} + \rho_0 \lambda (\theta - \theta_m) g - \frac{\nu H(x) \mu_f}{K(x)} u - \sigma_{nf} \beta_1^2 u = 0 \quad (1)$$

$$K_{nf} \frac{d^2\theta}{dx^2} + 2\beta_d \left(\frac{du}{dx} \right)^4 + \mu_{nf} \left(\frac{du}{dx} \right)^2 - \frac{dq}{dx} + \frac{\nu H^2(x) \mu_f}{K(x)} u^2 + \sigma_{nf} \beta_1^2 u^2 = 0 \quad (2)$$

subject to the boundary conditions below:

$$\begin{cases} u = 0, \theta = \theta_1 & \text{at } x = -h, \\ u = 0, \theta = \theta_2 & \text{at } x = h \end{cases} \quad (3)$$

Rosseland approximation is used for the calculation of radiative heat flux:

$$q = \frac{4\sigma^* \partial \theta^4}{3k^* \partial x} \quad (4)$$

where k^* and σ^* are mean absorption coefficient and Stephan-Boltzmann constant. By Taylor series for the expansion of temperature differences within the flow and neglecting terms of higher-order; radiative heat flux reduced to

$$q = -\frac{16\theta_\infty^3 \sigma^*}{3k^*} \frac{\partial \theta}{\partial x} \quad (5)$$

The following terms are expressed in term of ϕ (Solid volume fraction):

$$\rho_{nf} = \rho_f (1 - \phi) + \rho_f \phi \quad (6)$$

$$\mu_{nf} = \frac{\mu_f}{(1 - \phi)^{2.5}} \quad (7)$$

$$(\rho C_p)_{nf} = (\rho C_p)_f (1 - \phi) + (\rho C_p)_s \phi \quad (8)$$

$$\frac{K_{nf}}{K_f} = \frac{K_s + 2K_f - 2\phi(K_f - K_s)}{K_s + 2K_f + \phi(K_f - K_s)} \quad (9)$$

where K_{nf} , ρ_{nf} , $(\rho C_p)_{nf}$, and μ_{nf} is the thermal conductivity, effective density, heat capacitance and effective dynamic viscosity for nanofluid.

Table 1: Water and nanoparticles thermal-physical properties (Hussein, 2022)

Material	$\rho(kg/m^3)$	$C_p(J/(Kg \cdot k))$	$K(w/m \cdot k)$	$\beta \times 10^5(k^{-1})$
Water	997.1	417.9	0.613	21
C_uO	8933	385	401	1.67

The following similarity variables are used to reduced equations (1)-(2) to ordinary differential equations in dimensionless form:

$$v = \frac{u}{u_0}, \quad \zeta = \frac{x}{h} \quad \text{and} \quad \vartheta = \frac{\theta - \theta_m}{\theta_1 - \theta_2} \quad (10)$$

The mean temperature $\theta_m = \frac{1}{2}(\theta_1 + \theta_2)$. According to Reddy (2017), variable permeability $H(x)$ and variable porosity $K(x)$ with respect to similarity variables are expressed as;

$$H(\zeta) = h_0(1 + d_1 e^\zeta) \quad (11)$$

$$K(\zeta) = k_0(1 + d_2 e^\zeta) \quad (12)$$

Therefore, using equations (5) and (10), equations (1)-(3) reduced to:

$$\frac{d^2v}{d\zeta^2} + 6\delta(1 - \phi)^{2.5} \left(\frac{dv}{d\zeta} \right)^2 \frac{d^2v}{d\zeta^2} + \vartheta - \sigma\alpha_1 h_0 \left(\frac{1+d_1 e^{-\zeta}}{1+d_2 e^{-\zeta}} \right) v - AH_b^2(1 - \phi)^{2.5}v = 0 \quad (13)$$

$$\left(1 + \frac{4}{3DN_d} \right) \frac{d^2\vartheta}{d\zeta^2} + \frac{2\delta EP_r}{D} \left(\frac{dv}{d\zeta} \right)^4 + \frac{EP_r}{D} (1 - \phi)^{-2.5} \left(\frac{dv}{d\zeta} \right)^2 + \frac{E\sigma P_r h_0^2}{D} \left(\frac{(1+d_1 e^{-\zeta})^2}{1+d_2 e^{-\zeta}} \right) v^2 + Jv^2 = 0 \quad (14)$$

The relevant boundary conditions are:

$$\left. \begin{array}{l} v = 0, \quad \vartheta = \frac{1}{2} \quad \text{at} \quad \zeta = -1 \\ v = 0, \quad \vartheta = -\frac{1}{2} \quad \text{at} \quad \zeta = 1 \end{array} \right\} \quad (15)$$

where $D = \frac{K_{nf}}{K_f}$ (magnetic field), $A = \frac{\sigma_{nf}}{\sigma_f}$, $\mu_{nf} = \frac{\mu_f}{(1-\phi)^{2.5}}$, $U_0 = \frac{\rho_0 \lambda g h^2 (\theta_1 - \theta_2)}{\mu_{nf}}$, $E = \frac{u_0^2}{c_f(\theta_1 - \theta_2)}$ (Eckert number), $\delta = \frac{\beta_d u_0^2}{\mu_f h^2}$ (Dimensionless non-Newtonian viscosity), $\sigma = \frac{vh^2}{k_0}$ (Local porous parameter), $\alpha_1 = \frac{\mu_f}{\mu_{nf}}$ (Ratio of viscosity), $H_b^2 = \frac{\sigma_f \beta_1^2 h^2}{\mu_f}$ (Harmann number), $J = \frac{A\sigma_f \beta_1^2 u_0^2 h^2}{D K_f (\theta_1 - \theta_2)}$ (Joule heating), $N_d = \frac{K_f k^*}{4\sigma^* \theta_\infty^3}$ (Radiation parameter), and $P_r = \frac{\mu_f C_f}{K_f}$ (Prandtl number)

The skin friction and Nusselt number are expressed as follows:

$$C_f = \left(\frac{dv}{d\zeta} \right)_{\zeta=-1} (1 - \phi)^{-2.5} + \frac{1}{3} \delta \left(\frac{dv}{d\zeta} \right)_{\zeta=-1}^3 \quad (16)$$

$$Nu = -\frac{K_{nf}}{K_f} \left(\frac{d\vartheta}{d\zeta} \right)_{\zeta=-1} = -D \left(\frac{d\vartheta}{d\zeta} \right)_{\zeta=-1} \quad (17)$$

Method of Solution

The collocation method, based on an assumed Legendre polynomial, serves as an effective technique for solving linear and nonlinear ordinary differential equations. Like other orthogonal polynomial methods, it demonstrates great flexibility and ensures high convergence accuracy. Its adaptability and efficiency make it a reliable approach for tackling a variety of differential equation problems. Equations (13) and (14) can be solved using Legendre polynomial given below;

$$v(\zeta) = \sum_{j=0}^N a_j Q_j(\zeta) \quad (18)$$

$$v(\zeta) = a_0 Q_0(\zeta) + a_1 Q_1(\zeta) + a_2 Q_2(\zeta) + a_3 Q_3(\zeta) + a_4 Q_4(\zeta) + \dots \quad (19)$$

substituting for $Q_j(\zeta)$ in Equation (19) gives;

$$v(\zeta) = a_0 + \zeta a_1 + (-1 + 2\zeta^2)a_2 + (-3\zeta + 4\zeta^3)a_3 + (1 - 8\zeta^2 + 8\zeta^4)a_4 + \left. \begin{aligned} & + (5\zeta - 20\zeta^3 + 16\zeta^5)a_5 + (-1 + 18\zeta^2 - 48\zeta^4 + 32\zeta^6)a_6 + \\ & (-7\zeta + 56\zeta^3 - 112\zeta^5 + 64\zeta^7)a_7 + (1 - 32\zeta^2 + 160\zeta^4 - 256\zeta^6 + 128\zeta^8)a_8 \\ & + (9\zeta - 120\zeta^3 + 432\zeta^5 - 576\zeta^7 + 256\zeta^9)a_9 + \dots \end{aligned} \right\} \quad (20)$$

Similarly;

$$\vartheta(\zeta) = b_0 + \zeta b_1 + (-1 + 2\zeta^2)b_2 + (-3\zeta + 4\zeta^3)b_3 + (1 - 8\zeta^2 + 8\zeta^4)b_4 + \left. \begin{aligned} & + (5\zeta - 20\zeta^3 + 16\zeta^5)b_5 + (-1 + 18\zeta^2 - 48\zeta^4 + 32\zeta^6)b_6 + \\ & (-7\zeta + 56\zeta^3 - 112\zeta^5 + 64\zeta^7)b_7 + (1 - 32\zeta^2 + 160\zeta^4 - 256\zeta^6 + 128\zeta^8)b_8 \\ & + (9\zeta - 120\zeta^3 + 432\zeta^5 - 576\zeta^7 + 256\zeta^9)b_9 + \dots \end{aligned} \right\} \quad (21)$$

The unknown coefficients in Equations (20) and (21); $a_0, a_1, a_2, a_3, a_4, \dots$ and $b_0, b_1, b_2, b_3, b_4, \dots$, are obtained using Equation (15) and the collocation points.

Results and Discussion

This research examines the effects of variable porosity and joule heating on the behaviour of a non-Newtonian nanofluid confined between two bounded plates. The governing equations are derived and subsequently solved using appropriate mathematical techniques. The findings are presented both graphically and in tabular form to illustrate the influence of key fluid parameters. To systematically analyze these effects, specific default parameter values are selected. They are $N_d = 1, P_r = 1, H_b = 1, E = 1, \delta = 1, h_0 = 0.1, \phi = 0.01, d_1 = 1.5, d_2 = 3.0, \sigma = 0.1, \alpha_1 = 0.1, J = 0.1$. These values serve as a baseline for understanding the impact of different fluid characteristics on the overall flow and heat transfer behaviour. This study is evaluated alongside the findings of other researchers, as presented in Tables 5 and 6; by setting $H_b = 3, N_d = 2, P_r = 6.2, E = 1, \phi = 0.01, \delta = 1, \sigma = 0, h_0 = 0, J = 0$, and $\alpha_1 = 0$. The tables demonstrate that the results obtained align perfectly with those of previous studies, indicating a high level of agreement and consistency, thereby reinforcing the reliability and validity of the findings.

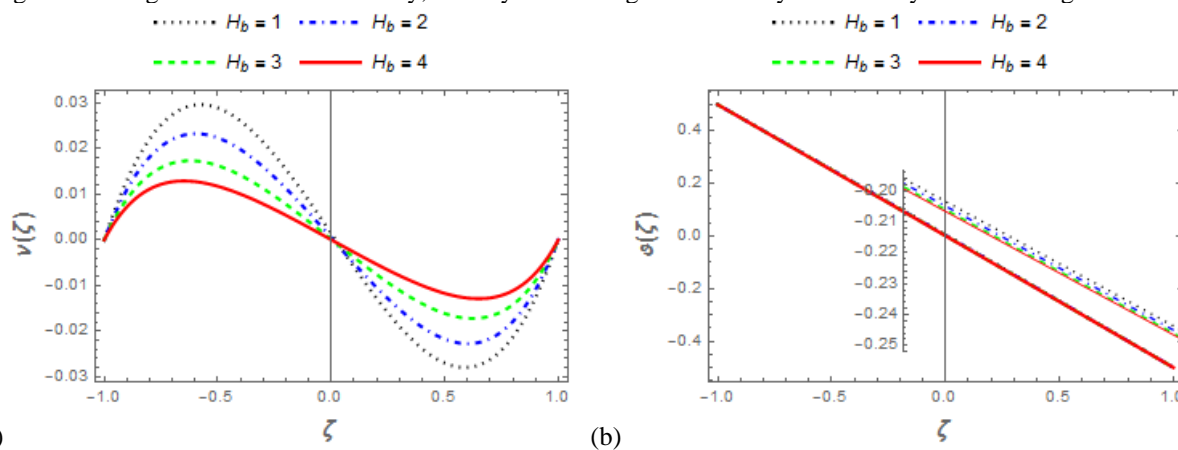


Figure 2: Velocity and Temperature profiles for values of H_b

Figure 2 presents the effects of the Hartmann number (H_b) on velocity and temperature profiles. The parameter H_b represents the influence of a magnetic field on the fluid's motion. Within the region $X = [-1, 0]$, velocity profile experienced decline due to a stronger magnetic field generating a higher Lorentz force, which resists the flow. Whereas, in region $X = [0, 1]$, the reverse is the case. The fluid experiences less magnetic drag, allowing the velocity to increase. This viscosity-induced variation in the non-Newtonian nanofluid alters the magnetic damping effect differently in each region. Figure 2b is an evidence of the fact that the fluid loses heat more efficiently near heated

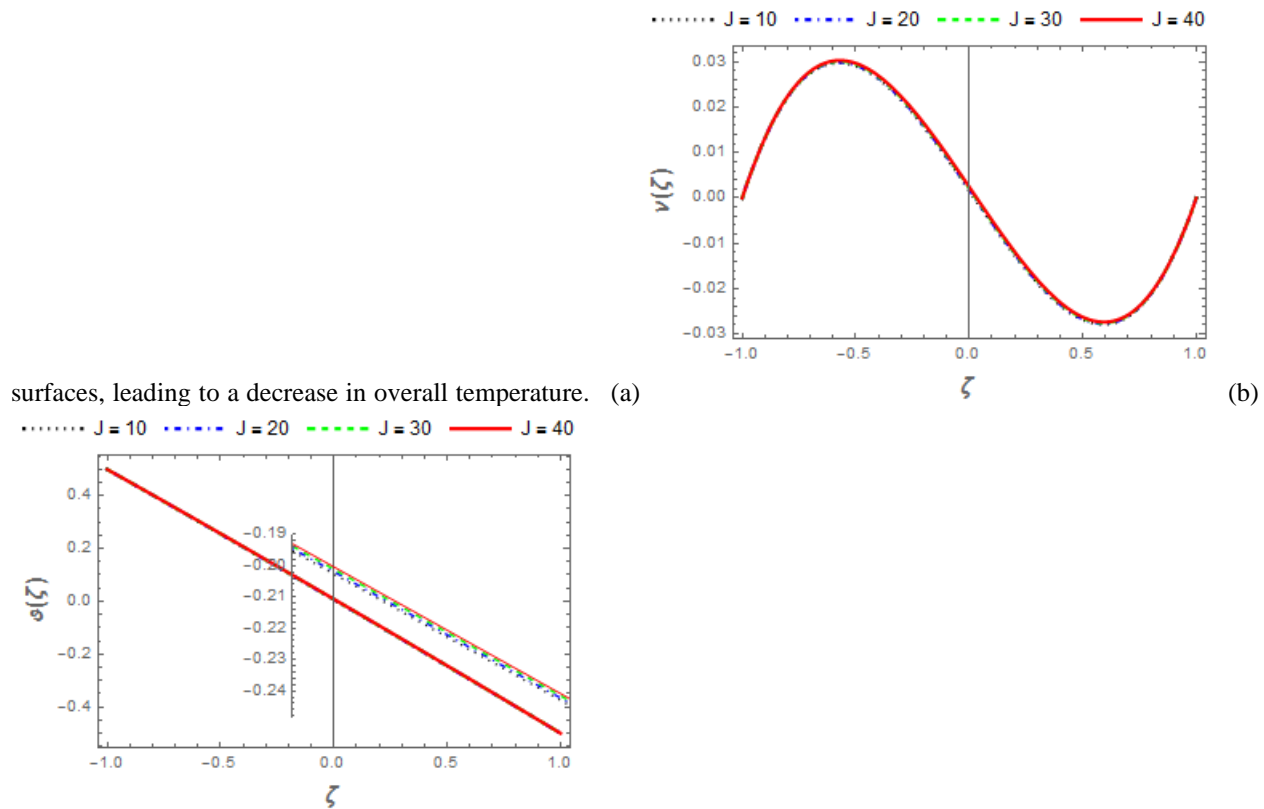
Figure 3: Velocity and Temperature profiles for values of J

Figure 3 illustrates the impact of Joule heating on velocity and temperature. Increased Joule heating accelerates fluid motion by lowering resistance and boosting convection, influencing applications such as MHD generators, plasma flows, and liquid metal cooling systems. In Figure 3b, the fluid temperature increases with increase in Joule heating. Higher Joule heating increases the fluid's electrical conductivity, resulting in stronger induced currents and a rise in fluid temperature.

Table 2: Values of Velocity for different values of J .

ζ	-1.0	-0.8	-0.6	-0.4	-0.2	0.0
$J = 10$	2.12511×10^{-18}	0.0218178	0.0289610	0.0252021	0.0144227	0.000231807
$J = 20$	2.44746×10^{-18}	0.0218932	0.0291065	0.0254005	0.0146523	0.000471382
$J = 30$	-1.97348×10^{-18}	0.0219776	0.0292690	0.0256219	0.0149082	0.000737924
$J = 40$	3.79633×10^{-18}	0.0220625	0.0294327	0.0258445	0.0151652	0.00100506
ζ	0.2	0.4	0.6	0.8	1.0	
$J = 10$	-0.0139817	-0.0248272	-0.0286899	-0.0216778	1.81461×10^{-18}	
$J = 20$	-0.0137528	-0.0246302	-0.0285457	-0.021603	-2.69097×10^{-18}	
$J = 30$	-0.0134987	-0.0244117	-0.0283859	-0.0215203	-9.00965×10^{-20}	
$J = 40$	-0.0132445	-0.0241934	-0.0282265	-0.0214378	6.08946×10^{-21}	

Table 3: Values of Temperature for different values of J

ζ	-1.0	-0.8	-0.6	-0.4	-0.2	0.0
$J = 10$	0.5	0.400297	0.300482	0.200643	0.100765	0.000811101

$J = 20$	0.5	0.400631	0.301075	0.20137	0.101527	0.00157114
$J = 30$	0.5	0.401007	0.301743	0.202187	0.10238	0.00241685
$J = 40$	0.5	0.401388	0.302421	0.203015	0.103241	0.00326463
ζ	0.2	0.4	0.6	0.8	1.0	
$J = 10$		-0.0992351	-0.199358	-0.29952	-0.399704	-0.5
$J = 20$		-0.0984825	-0.198646	-0.298941	-0.39938	-0.5
$J = 30$		-0.0976505	-0.197862	-0.298306	-0.399024	-0.5
$J = 40$		-0.0968222	-0.197086	-0.297678	-0.398673	-0.5

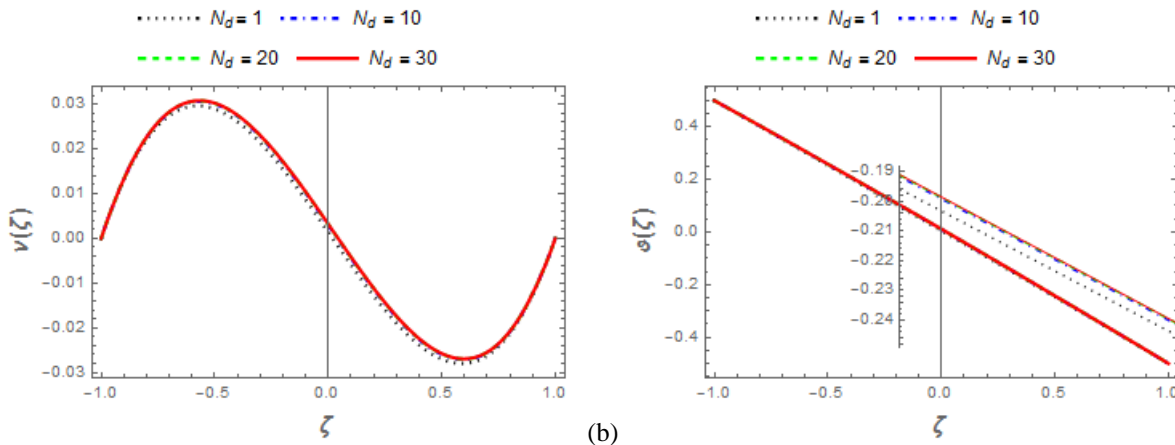
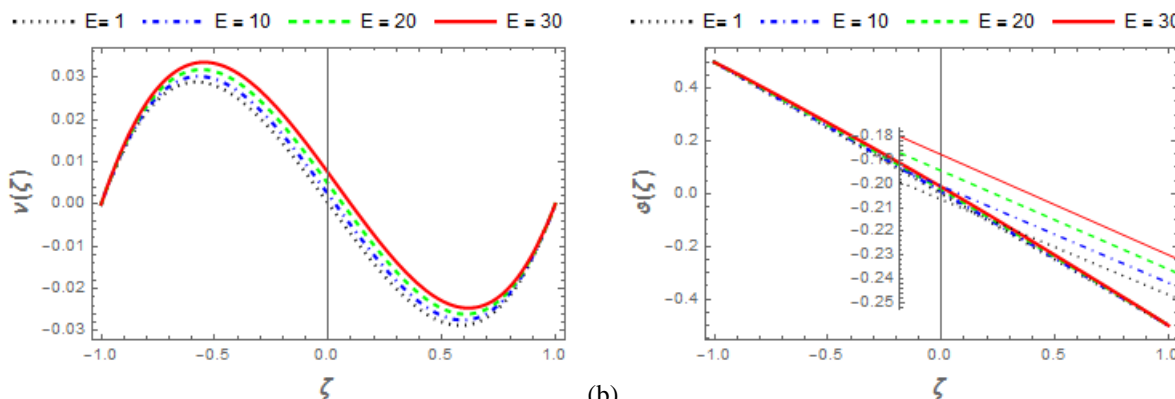
Figure 4: Velocity and Temperature profiles for values of N_d

Figure 4a and 4b show the impact of radiation on velocity and temperature. Both velocity and temperature profiles accelerate with higher values of radiation parameter. A higher radiation parameter strengthens thermal radiation effects, increasing fluid temperature and lowering viscosity in temperature-sensitive fluids, which enhances velocity. Elevated radiation levels improve heat transfer, expanding the thermal boundary layer and stabilizing the temperature profile. The interplay of reduced viscosity and intensified heat transfer amplifies convection, accelerating fluid motion. This phenomenon is crucial in high-temperature systems such as astrophysical flows, nuclear reactors, and thermal insulation, where radiation significantly influences heat and momentum transport.

Figure 5: Velocity and Temperature profiles for values of E

In Fig. 5, it can be seen that with a higher Eckert number, more kinetic energy is converted into internal energy due to viscous friction within the fluid. This increased energy input raises the fluid temperature, directly affecting its

rheological properties and flow behaviour. Furthermore, as E increases, the resulting temperature rise reduces viscosity, lowering heat dissipation rates and trapping more energy within the fluid, which further increases the temperature.

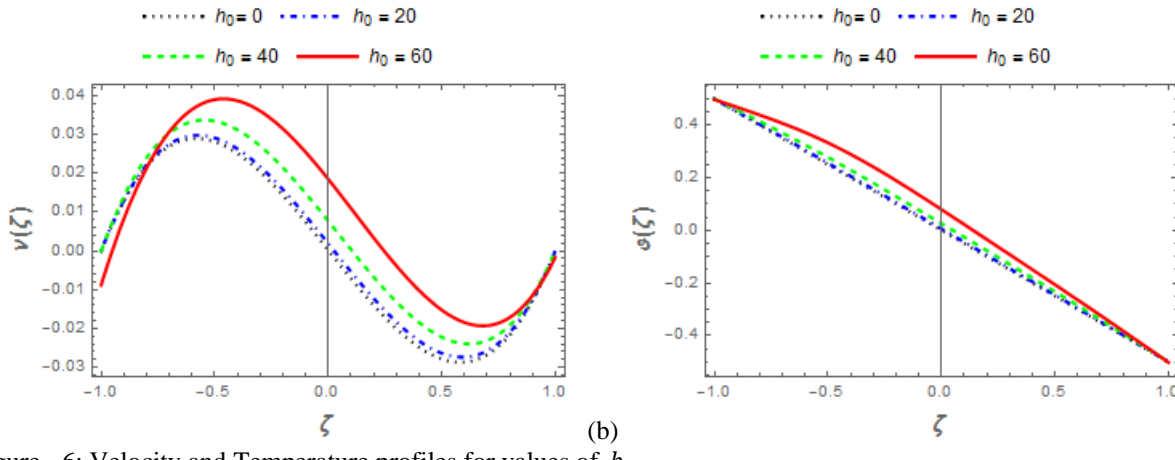


Figure 6: Velocity and Temperature profiles for values of h_0

Figure 6 illustrates the impact of h_0 on both velocity and temperature. A porous boundary facilitates momentum exchange between fluid layers, enhancing interaction and momentum diffusion. This results in a more uniform velocity profile and an overall increase in fluid velocity. As shown in Figure 6b, increased porosity alters the thermal boundary layer, reducing its thickness. Consequently, a thinner thermal boundary layer enhances thermal gradients, increasing heat retention within the fluid and raising the overall temperature.

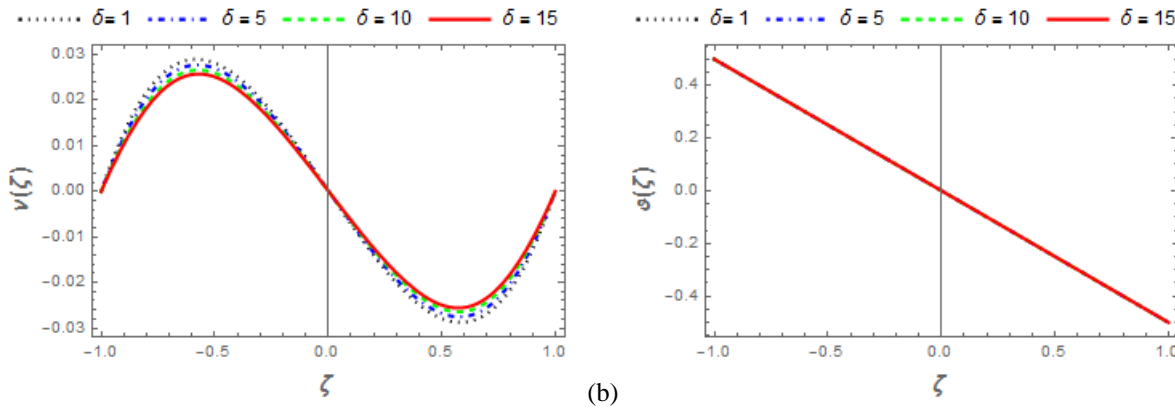


Figure 7: Velocity and Temperature profiles for values of δ

Table 4: Values of Temperature for different values of δ

ζ	-1.0	-0.8	-0.6	-0.4	-0.2	0.0
$\delta = 1$	0.5	0.400264	0.300423	0.200571	0.100689	0.000735130
$\delta = 5$	0.5	0.400253	0.300404	0.200544	0.100656	0.000699581
$\delta = 10$	0.5	0.400244	0.300388	0.200520	0.100627	0.000668089
$\delta = 15$	0.5	0.400236	0.300375	0.200502	0.100605	0.000644092
ζ	0.2	0.4	0.6	0.8	1.0	
$\delta = 1$	-0.0993106	-0.199429	-0.299578	-0.399737	-0.5	
$\delta = 5$	-0.0993436	-0.199456	-0.299596	-0.399748	-0.5	
$\delta = 10$	-0.0993729	-0.19948	-0.299613	-0.399757	-0.5	
$\delta = 15$	-0.0993953	-0.199498	-0.299626	-0.399765	-0.5	

Figure 7a and 7b depict the influence of δ on velocity and temperature respectively. With high viscosity, the overall momentum transport is hindered, slowing the flow. Velocity profiles shows that viscosity decreases in some regions and remains high in others, hence velocity gradients is sharper near the walls.

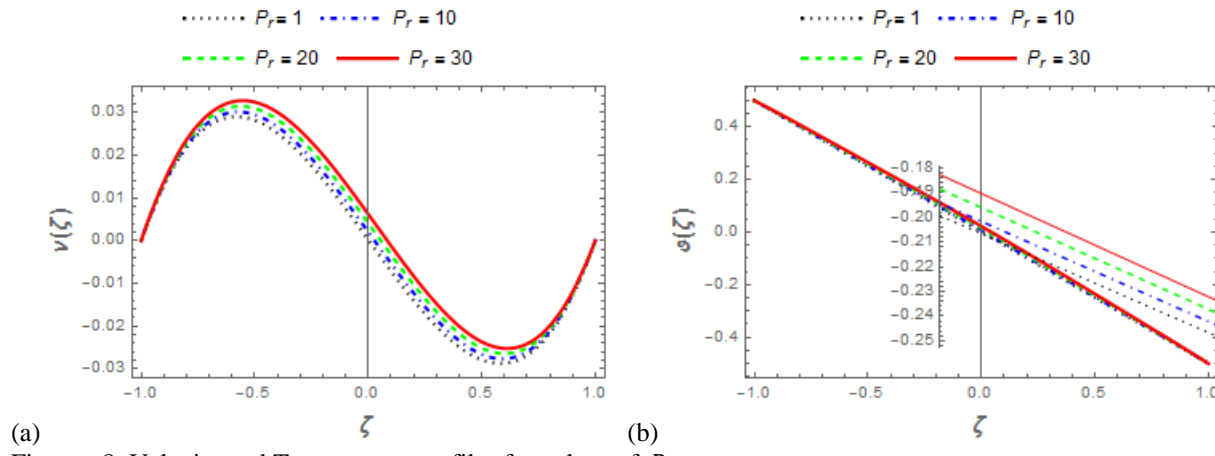


Figure 8: Velocity and Temperature profiles for values of P_r

The effects of P_r on v and θ is presented in figure 7a and 7b. Velocity and temperature profiles increase with increase in P_r . A higher Prandtl number (P_r) increases momentum diffusivity relative to thermal diffusivity, resulting in a thinner thermal boundary layer and sharper temperature gradients. Reduced thermal diffusion strengthens temperature profiles, while greater viscosity effects constrain flow near surfaces, refining the velocity profile. This leads to steeper velocity gradients and heightened shear stress. The impact is crucial in heat exchangers, cooling systems, and high- P_r fluids like oils, where precise heat and momentum control enhances efficiency.

Table 5: Comparison: Values of $v(\zeta)$ for solution by shooting method, FDM, and MDTM with the present work when $H_b = 3$, $N_d=2$, $P_r = 6.2$, $E = 1$, $\phi = 0.01$, $\delta = 1$, $\sigma = 0$, $h_0 = 0$, $J = 0$, and $\alpha_1 = 0$.

ζ	Hussein (2022) $v(\zeta)$			Present work $v(\zeta)$
	MDTM	FDM	Shooting method	LCM
-1	0	0	0	0
-0.9	0.008927973453246	0.008787225412899	0.008957094	0.008970846
-0.8	0.014223686772939	0.013959477936244	0.014244837	0.014302614
-0.7	0.01676965479026	0.016440045972315	0.016784495	0.016871717
-0.6	0.017266325478027	0.016922743531933	0.017251388	0.017378822
-0.5	0.016255425114184	0.015931229672889	0.016188057	0.016366036
-0.4	0.014150728407177	0.013863775889415	0.014023246	0.014247972
-0.3	0.011268952330109	0.011027308517539	0.011090881	0.011343070
-0.2	0.007857588237348	0.007663635866098	0.007649044	0.007900498
-0.1	0.004116729433862	0.003970101131019	0.003898955	0.004122128
0	0.000217343161713	0.000116424993575	0.000039459	0.000180547
.1	-0.0036832980283544	-0.003740824702763	-0.003891557	-0.003765548
.2	-0.007427456163251	-0.007444902635067	-0.007643058	-0.007557283
.3	-0.010842771287347	-0.010825560149113	-0.011087014	-0.011021553
.4	-0.013726806197571	-0.013684591023138	-0.014021855	-0.013955725
.5	-0.015828922831118	-0.015779021734224	-0.016189006	-0.016109755
.6	-0.016828099926917	-0.016800520671318	-0.017253911	-0.017164390

.7	-0.016305660627378	-0.016349281399216	-0.016787055	-0.016704424
.8	-0.0137132512402211	-0.013900167871314	-0.014244981	-0.014187391
.9	-0.0083405628843889	-0.008758254914885	-0.008951319	-0.008912075
	0.000703069482021	0	0	0

Table 6: Comparison: Values of $\vartheta(\zeta)$ for solution by shooting method, FDM, and MDTM with the present work when $H_b = 3$, $N_d = 2$, $P_r = 6.2$, $E = 1$, $\phi = 0.01$, $\delta = 1$, $\sigma = 0$, $h_0 = 0$, $J = 0$, and $\alpha_1 = 0$

ζ	Hussein (2022) $\vartheta(\zeta)$			Present work $\vartheta(\zeta)$
	MDTM	FDM	Shooting method	
-1	0.5	0.5	0.5	0.5
-0.9	0.45048334393744	0.4500557057	0.449970142	0.450478298
-0.8	0.400767395390827	0.40020133769	0.399959597	0.400759848
-0.7	0.350989746391596	0.35039626873	0.349957975	0.350980173
-0.6	0.301201167815963	0.30061028898	0.299961713	0.301189619
-0.5	0.251410810147527	0.25082103146	0.249968222	0.251397309
-0.4	0.201610063585561	0.20101206823	0.199975753	0.201594752
-0.3	0.151784736266043	0.15117151419	0.149983257	0.151767849
-0.2	0.101920941655585	0.10129101917	0.099990246	0.101902741
-0.1	0.052007749159865	0.05136506198	0.049996659	0.051988479
0	0.002038317205475	0.00139048604	0.000002718	0.002018162
.1	-0.04798969711509	-0.04863376327	-0.049991207	-0.048010640
.2	-0.09807401948685	-0.09870672228	-0.099984735	-0.098095756
.3	-0.14820784031401	-0.14882532079	-0.149977617	-0.148230500
.4	-0.19838020932551	-0.19898411506	-0.199969867	-0.198404058
.5	-0.24857715789604	-0.24917481927	-0.249961909	-0.248602577
.6	-0.29878442328292	-0.29938559613	-0.299954708	-0.298811805
.7	-0.3489934561497	-0.34960004659	-0.349949910	-0.349022883
.8	-0.3992138754586	-0.39979581311	-0.399949984	-0.399244297
.9	-0.4494979788967	-0.44994267864	-0.449958355	-0.449525327
	-0.4999868653492	-0.5	-0.5	-0.5

Table 7: Skin Friction and Nusselt number for different fluid parameters

J	h_0	H_b	N_d	P_r	δ	E	ϕ	S_f	Nu
0.1	0.1	1	1	1	1	1	0.01	0.156053763	0.518222071
0.5								0.156113096	0.517946376
0.5								0.156036116	0.518214040
2								0.135630878	0.518951373
		2						0.156177765	0.517402057
			10					0.158882772	0.498985288
				5				0.142835153	0.51832710
					10			0.158882772	0.498985288
						0.04		0.169972900	0.584063750

Table 7 presents the effects of $J, P_r, E, \phi, h_0, \delta, H_b$ and N_d on the system. An increase in N_b, P_r, E, ϕ , and J led to higher skin friction, while h_0, δ and H_b caused a reduction. Likewise, the heat transfer coefficient increased with rising values of H_b, δ and ϕ .

Conclusion

The influence of variable Porosity and permeability on the flow characteristics and heat transfer in Non-Newtonian nanofluid is considered. With the incorporation of effects of MHD, the impacts of various fluid properties like H_b, J, N_d , and E_c are examined on both velocity and temperature profiles. The results revealed the relationship between the thermophysical factors and the porous medium structural characteristics by displaying it significant on heat transfer and the movement of the fluid.

Among other results, one of the significant results is evidence; the increase in H_b retards velocity profiles as a result of impact of improved Lorentz force. While R and J accelerate thermal energy of the nanofluid. Finally, permeability and porosity variation cause a kind of resistance of the fluid motion. These results are relevant and useful for optimizing technologies in the area of cooling by utilizing nanofluids and industrial processes involving high temperature where proper thermal control is important. This work reveals the relationship between porous medium, heat transfer and fluid flow, hence provides insights in improvement and design of thermal systems.

Disclosure Statement: There is no conflict of interest reported by the authors.

References

Agunbiade, S. A., & Dada, M. S. (2019). Effects of viscous dissipation on convective rotatory chemically reacting Rivlin-Ericksen flow past a porous vertical plate. *Journal of Taibah University for Science*, 13(1), 402-413. <https://doi.org/10.1080/16583655.2019.1582149>

Agunbiade, S. A., Oyekunle, T. L., & Akolade, M. T. (2023). Radiative and MHD Dissipative heat effects on Upper-convected Maxwell fluid flow and material time relaxation over a permeable stretched sheet. *Computational Thermal Sciences*, 15 (3), 45-59.

Amel, A. A., & Mohamed, R. E. (2020). 3-D electromagnetic radiative non-Newtonian nanofluid flow with Joule heating and higher-order reactions in porous materials. *Scientific Reports*, (2020) 1014513. doi.org/101038/s41598-020-71543-4

Anas A.M., Arafa, Z. Z., & Sameh E. A. (2021). Radiative flow of non-Newtonian nanofluids within inclined porous enclosures with time fractional derivative. *Scientific Reports* (2021) 11,5338. <https://doi.org/10.1038/s41598-021-84848-9>

Asia, A. A., Aziz, U. A., Shafiullah, N., Sohail, N., Ameer, A. A., Roobaea, A., Hanadi, A., & Fehmi, G. (2024). Radiation-influenced magnetohydrodynamic third-grade Nanofluid flow around non-linearly stretched cylinder. *Journal of Computational Design and Engineering*, 2024, 11,72-90. DOI:10.1093/jcde/qwae038

Ayub, R., Ahmad, S., & Ahmad, M. (2022). MHD rotational flow of viscous fluid past a vertical plate with slip and Hall effects through porous media: A theoretical modeling with heat and mass transfer. *Advances in Mechanical Engineering*, 14(6), 1-14. DOI: 10.1177/16878132221103330

Bidyut, M., Krishnendu, B., Astick, B., Ajeet, K. V., & Anil, K. G. (2020). MHD mixed convection on an inclined stretching Plate in Darcy porous medium with Soret effect and variable surface conditions. *De Druyter*, 2020 (9), 457-469. <https://doi.org/10.1515/nleng-2020-0029>

Hassana, M., Marinb, M., Alsharif, A., & Ellahi, A. (2018). Convective heat transfer flow of nanofluid in a porous medium overwavy surface. *Elsevier B.V.*, (2018), 0375-9601 <https://doi.org/10.1016/j.physleta.2018.06.026>

Hussein, A. S. (2022). Radiative MHD flow of Rivlin-Ericksen nanofluid of grade three through porous medium with uniform heat source. *Beni-Suef University Journal of Basic and Applied Sciences*, (2022) 11,81. <https://doi.org/10.1186/s43088-022-00261-9>

Jha B. K., & Ajibade A. O.(2015). Transient natural convection flow between vertical parallel plates: one plate isothermally heated and the other thermally insulated. *J. Process Mechanical Engineering*, 224, 247-251.

Karem, M. E., & Hussein A. S. (2022). MHD Natural Convection Nanofluid Flow between Two Vertical Flat Plates through Porous Medium Considering Effects of Viscous Dissipation, non-Darcy, and Heat Generation/Absorption. *International Journal of Advanced Engineering and Business Sciences (IJAEBs)*, 4 (3), 126-142. DOI:10.21608/ijaeb.2022.157903.1031

Khan, N. S., Sriyab, S., Kaewkhao, A., & Thawinan, E. (2022). Hall current effect in bioconvection Oldroyd-B nanofluid flow through a porous medium with Cattaneo-Christov heat and mass flux theory. *Scientific Reports*, (2022) 12,19821. <https://doi.org/10.1038/s41598-022-23932-0>

Oyekunle, T. L., Akolade, M. T., Agunbiade, S. A., & Adeniran, P. O. (2023). (R2058) MHD Stagnation Point Flow of Nanofluid with Buoyancy Effect Through a Porous Shrinking Sheet. *Applications and Applied Mathematics: An International Journal (AAM)*, 19 (1),1-15. <https://digitalcommons.pvamu.edu/aam/vol19/iss1/>

Peyman. M., Gholamreza, S., Hamed, R., & Sadegh, S. (2019). Flow and natural convection heattransfer characteristics of non-Newtonian nanofluid flow bounded by two infinite vertical flat plates in presence of magnetic field and thermal radiation using Galerkin method. *J. Cent. South Univ.*, (2019) 26, 1294–1305. DOI: <https://doi.org/10.1007/s11771-019-4088-5>

Rajagopal, K. R., Pittsburgh, P., & Dearborn, M. T. Y. (1985). Natural Convection Flow of a Non-Newtonian Fluid Between Two Vertical Flat Plates. *Acta Mechanica*, 54, 239–246.

Rajdeep B., Nazibuddin A., & Kalyan C. (2023). Free Convective MHD Radiative Flow Past a Porous Vertical Plate in a Porous Medium with Chemical Reaction. *Biointerface Research in Applied Chemistry*, 13 (3),1-15. <https://doi.org/10.33263/BRIAC133.259>

Reddy, G. M., Dinesh, P. A., & Sandeep, N. (2017). Effects of variable viscosity and porosity of fluid, Soret and Dufour mixed double diffusive convective flow over an accelerating surface. *IOP Conf. Series: Materials Science and Engineering*, 263(2017),062012. doi:10.1088/1757-899X/263/6/062012

Subbarao, A., Anwar, B. A., & Ramachandra, P. V. (2016). Thermal radiation effects on non-Newtonian fluid in a variable porosity regime with partial slip. *Journal of Porous Media*, 19 (4). 1-17. DOI: 10.1615/JPorMeda.v19.i430

Verma, A. K., Gautam, A. K., Bhattacharyya, K., & Sharma, R. P. (2021). Existence of boundary layer nanofluid flow through a divergent channel in porous medium with mass suction/injection. *Sadhana* (2021) 46,98. <https://doi.org/10.1007/s12046-021-01588-2>

Zayyanu, S. Y., Musa, A. K., Gatawa, A. M., Hassan, I. K., & Hussaini, A. (2022). Effects of Porosity on Free Convection between Vertical Walls with Point/Line Heat Source/Sink. *Saudi Journal of Engineering and Technology*, 7(6), 343-347. DOI: 10.36348/sjet.2022.v07i06.010

Appendix

Nomenclature

u, v	dimensional velocity components in the x and y directions respectively (m / s)
x, y	direction coordinate of velocity (m)
C_f	specific heat ($J \ k \ g^{-1} K^{-1}$)
P_r	Prandtl number
H_b	Hartmann number
g	gravity (m / s^2)
N_d	radiation parameter
E	Eckert number
q	radiative heat flux
nf	Nanofluid
K_f	thermal conductivity of the fluid
K_{nf}	thermal conductivity of nanofluid
s	solid
h	dimensional distance between the two plates (m)
h_0	boundary layer edge porosity

K_0	boundary layer edge porosity
d_1 d_2	variable permeability constants
J	Joule heating
f	fluid
D	magnetic field
Greek Symbols	
v	non-dimensional velocity components in the ζ directions
μ_{nf}	dynamic viscosity of nanofluid
ρ_{nf}	density of the fluid (k g m^{-3})
λ	coefficient of thermal expansion(K^{-1})
ϕ	Nanofluid volume fraction
ζ	dimensionless form of distance
ϑ_1, ϑ_2	temperature at the wall (K)
ϑ_m	mean temperature
ϑ	dimensionless temperature
σ_{nf}	electrical conductivity
ρ_0	a constant
β_d	temperature function of material modules
μ_f	dynamic viscosity of the fluid
σ	parameter of local porosity
δ	non-Newtonian viscosity in dimensionless form
β_1	magnetic induction (tesla)